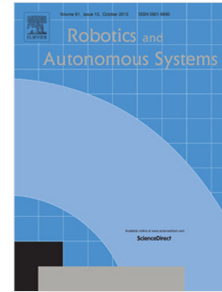


# Accepted Manuscript

Neural network for black-box fusion of underwater robot localization under unmodeled noise

Hendry Ferreira Chame, Matheus Machado dos Santos, Sílvia Silva da Costa Botelho



PII: S0921-8890(18)30292-6  
DOI: <https://doi.org/10.1016/j.robot.2018.08.013>  
Reference: ROBOT 3075

To appear in: *Robotics and Autonomous Systems*

Received date : 6 April 2018  
Revised date : 7 August 2018  
Accepted date : 31 August 2018

Please cite this article as: H.F. Chame, et al., Neural network for black-box fusion of underwater robot localization under unmodeled noise, *Robotics and Autonomous Systems* (2018),  
<https://doi.org/10.1016/j.robot.2018.08.013>

This is a PDF file of an unedited manuscript that has been accepted for publication. As a service to our customers we are providing this early version of the manuscript. The manuscript will undergo copyediting, typesetting, and review of the resulting proof before it is published in its final form. Please note that during the production process errors may be discovered which could affect the content, and all legal disclaimers that apply to the journal pertain.

# Neural network for black-box fusion of underwater robot localization under unmodeled noise

Hendry Ferreira Chame<sup>1\*</sup>, Matheus Machado dos Santos<sup>1</sup>, Sílvia Silva da Costa Botelho<sup>1</sup>

---

## Abstract

The research on autonomous robotics has focused on the aspect of information fusion from redundant estimates. Choosing a convenient fusion policy, that reduces the impact of unmodeled noise, while being computationally efficient, is an open research issue. The objective of this work is to study the problem of underwater localization which is a challenging field of research, given the dynamic aspect of the environment. For this, we explore navigation task scenarios based on inertial and geophysical sensory. We propose a neural network framework named B-PR-F which heuristically performs adaptable fusion of information, based on the principle of contextual anticipation of the localization signal within an ordered processing neighborhood. In the framework black-box unimodal estimations are related to the task context, and the confidence on individual estimates is evaluated before fusing information. A study conducted in a virtual environment illustrates the relevance of the model in fusing information under multiple task scenarios. A real experiment shows that our model outperforms the Kalman Filter and the Augmented Monte Carlo Localization algorithms in the task. We believe that the principle proposed can be relevant to related application fields, involving the problem of state estimation from the fusion of redundant information.

*Keywords:* Robot localization, Neural networks, Underwater robotics,

---

\*Corresponding author: Hendry Ferreira Chame

<sup>1</sup>Universidade Federal do Rio Grande (FURG), Programa de Pós-Graduação em Modelagem Computacional, Centro de Ciências Computacionais C3, Grupo NAUTEC, Rio Grande, RS, Brazil. E-mail: {hendrychame, matheusmachado, silviacb}@furg.br

**Information fusion**

*2010 MSC:* 68T40, 68T05, 68T20, 93C85, 93C10

**1. Introduction**

Localization in underwater environments is a challenging field of study with interesting research topics. Depending on the autonomy of the vehicle two categories of robots are available: *autonomous underwater vehicle* (AUV) and *remotely operated vehicle* (ROV). An AUV, also known as *unmanned underwater vehicle*, is designed for autonomous functioning with minor or no intervention from the surface operator. According to Pauli et al. [1], AUV designs include diverse shapes (e.g. torpedo, gliders, hovercraft, among others), with sizes ranging from small human portable to heavy equipment (in the order of tons of weight). ROVs are unoccupied underwater robots connected to the surface by cables, so they can transmit the command and control signals between the operator and the robot. Conforming to Grøtli et al. [2], ROVs are largely employed for subsea inspection, maintenance, and repair operations.

Despite terrestrial localization has been widely studied, available techniques cannot be directly applied to underwater scenarios, due to diverse challenges associated to these environments (e.g. the rapid attenuation of higher frequency signals, and the unpredictable nature of the environment, Tan et al. [3]). Underwater vehicles are equipped by a variety of sensors (e.g. acoustic, vision, velocity, accelerometers, and gyroscopes sensors), providing information on the robot's position and movement. Though, according to Luo et al. [4], acoustic sensors are more commonly used. In any case, an important aspect of research consists in designing algorithms for sensory information fusion, so the heterogeneous data acquired by the robot, under different conditions, can be coherently combined, in order to provide an estimate on the localization of the vehicle in relation to an established reference frame.

Depending on the sensory technology or data processing algorithms employed, it is normally the case that observations can be compared based on sev-

eral properties, including: efficiency, operation rate, reliability, accuracy, availability, or other cost functions. Acoustic positioning sensory are, for instance, subject to intermittence (i.e. they provide asynchronous measurements), and larger noise levels over short time periods, but estimates do not drift over time. Thus, at the long run measurements can be more reliable than on-board dead reckoning estimates (Drolet et al. [5]). Analogously, the recognition of fixed geo-referenced landmarks can be more informative on the robot position than acoustic global estimates, though the robot may have to surface in order to reduce the localization uncertainty, given that the vehicle cannot receive the global positioning system (GPS) radio frequency in the underwater medium (Khan et al. [6]).

Bayesian fusion algorithms, such as the Kalman Filter (KF) family, are very popular in the field (e.g. in Botelho et al. [7], and Potyagaylo [8]). However, by holding the assumption of a Gaussian distribution of noise, the algorithm performs poorly when the estimation process deals with un-modeled noise. Unfortunately, this is likely to happen in natural underwater environments, affecting the quality of the obtained estimates. Non-parametric algorithms, such as particle filters (e.g. Monte Carlo localization or MCL, Thrun et al. [9]), produce a global estimate from multi-modal hypotheses, which can handle unmodeled noise. However, MCL is often computationally expensive, and exhibit non-optimal performance in situations close to a Gaussian distribution of noise. Consequently, the problem of improving unimodal estimates under non-Gaussian noise has been of concern.

When studying the localization problem as a KF fusion process, one approach that is often reported in the literature is to model non-linearities by augmenting the state representation (e.g. in Morgado et al. [10]). When such knowledge is difficult to be obtained, an alternative has been resorting to supervised learning methodologies for training the fusion algorithm in correcting the estimates (e.g. in Gao et al. [11]). An inconvenience associated to the latter approach, in relation to dynamic environments, is the fact of relying on the assumption that the task conditions will not vary significantly between the

training and the execution steps.

Some works have proposed to perform the fusion of redundant estimations viewed as black-box processes. Thus, a strategy adopted has been to weight the contribution of each estimate based on the information provided by the error covariance matrix (e.g. by weighting inversely proportionally in Drolez et al. [5], or the *covariance intersection* approach in Julier & Uhlmann [14]). However, in the fusion process correction measurements are implicitly assumed to follow Gaussian distributions. Alternatively, knowledge relative to the fusion process has been represented as a fuzzy rule-based system (Sabra & Fung [13]). Thus, more complex fusion scenarios can be modeled by the system designer.

Under certain circumstances, in particular with AUVs, acoustic positioning systems can present additional challenges to sensory fusion algorithms. This is the case, for instance, when data is sent to the robot by modem, and may arrive delayed to the fusion algorithm. According to Gopalakrishnan et al. [14], methods that handle this condition can be categorized into two groups: those that fuse the delayed measurements on arrival (e.g. in Ridao et al. [15]), and those that resort to state augmentation to model delays (e.g. in Asadi & Bottasso [16]). For the case of ROVs, the robot is umbilically connected to sea surface, so the problem of delayed fusion is generally mitigated.

Differently from the works by Morgado et al. [10] and Gao et al. [11], which have treated the aspect of modeling or acquiring knowledge about the task dynamics, the focus of our research was placed on a higher level of abstraction. In this sense, we have adopted an approach closer to the work by Sabra & Fung [13], by acknowledging the importance of identifying different situations encountered in the navigation task, which conditions the relevance of available estimates for the fusion process. However, our research has mainly focused on developing an heuristic and generic policy for evaluating the information provided by redundant estimators, in order to obtain a fusion process that can reliably handle unmodeled noise.

Concretely, we propose an architecture where redundant localization estimation nodes are viewed as black-box processes. The information fusion step

is performed by a neural network structure named B-PR-F, that is designed to exploit the principle of contextual information anticipation for obtaining a more reliable fusion, which has been adopted in a previous work by Chame & Chevallereau [17] for egocentric localization and visual attention. In B-PR-F an ordering arrangement is established, so the reliability of nodes' estimates is evaluated within a processing neighborhood. Thus, estimates' mean value and the expected deviation are anticipated by related neighbors. The confidence is evaluated within the context of the task, and the nodes' contributions to the global estimation are accordingly weighted in the fusion step.

The remaining of this document is organized as follows. In Sec. 2 the framework proposed is detailed, along with the neural network structure B-PR-F. In Sec. 3 the materials and methods considered are described, including the simulation environment and the experiment. A ROV architecture equipped with the compass, the *ultra-short baseline* (uSBL), and the *sound navigation and ranging* (SONAR) sensors was employed. In Sec. 4 the evaluation conducted in the virtual environment is reported, so the performance of the framework is studied under two distinct navigation task scenarios. Section 5 reports on the localization task executed in the real experiment, in which the method proposed is compared to the KF and the Augmented MCL approaches. In Sec. 7 the results obtained are discussed. Finally, in Sec. 8 the conclusions are presented and future perspectives are discussed.

**Notation** Matrix variables are denoted by bold capital letters  $\mathbf{A}$ , vector variables are denoted by low-case bold letters  $\mathbf{a}$ . The dimension of vectors and matrices is indicated within sub-script brackets (e.g.  $\mathbf{A}_{[p \times q]}$  is of dimension  $p \times q$ ). The terms  $\mathbf{I}_{[n]}$ ,  $\mathbf{1}_{[n]}$ , and  $\mathbf{0}_{[n]}$  represent respectively the  $n \times n$  identity matrix, the matrix of ones, and the matrix of zeros. The transpose of a matrix or a vector is denoted by  $(\top)$  (e.g.  $\mathbf{a}^\top$ ). Sub-script indexes denote elements in a matrix or vector, for instance the  $ij^{\text{th}}$  element of matrix  $\mathbf{A}$  is denoted by  $\mathbf{A}_{ij}$ . The operator  $(:)$  is used in case complete rows or columns are queried, thus  $\mathbf{A}_1$  would denote the first column of  $\mathbf{A}$ .  $\|\mathbf{a}\|_1 = \sum_{i=1}^n |\mathbf{a}_i|$  is the  $\ell_1$  norm

for a  $n$ -dimensional real vector space.  $\|\mathbf{A}\|_2 = \sqrt{\sum_{i,j} \mathbf{A}_{ij}^2}$  is the Frobenius norm. Functions are denoted by low-case letters. Parameters are enclosed in parenthesis (e.g. the function  $f(s)$  would depend on parameter  $s$ ). Variables dependence is shown in sub-script style (e.g. the matrix  $\mathbf{A}_{(t)}$  would depend on variable  $t$ ). The indexing of a family of functions or parameters is denoted by low-case subscripts (e.g. a function  $f_c(t)$  would be a particular instance of a family of related functions  $c \in C$ ). Superscripts are used to improve readability of weight matrices, thus  $\mathbf{W}^{PR}$  would denote the weight matrix connecting layers P and R in the network.

## 2. Theory/calculation

The framework proposed is designed under the principle that several localization algorithms are available to the system in different tasks conditions, so the main goal of the fusion algorithm is to dynamically consider their relative advantages. Figure 1 illustrates the architecture proposed. A set of sensor measurements in gray boxes are passed to the yellow containers, through the system bus. These nodes encapsulate individual estimation processes. The blue node includes the fusion algorithm, which weights the contribution of the estimators in the fusion process.

The reset feature is an important aspect of the architecture design. Thus, the fusion node is also in charge of firing a signal with the available global estimate, so the yellow nodes can be re-initialized under reliable circumstances. This is cardinal for reducing the accumulation of errors within certain estimator nodes. In this sense, under the adequate circumstances, a node encapsulating a dead reckoning localization algorithm could be provided with a fix from the global estimate. The reset signal is also important to ensure context transitions occurring in the task as the scenarios encountered vary. The model's premises are detailed next.

Let an estimator process  $i \in I$  provide information at time  $t$  on the system's continuous state through the parameters set  $\Psi_{i(t)}$ , such that

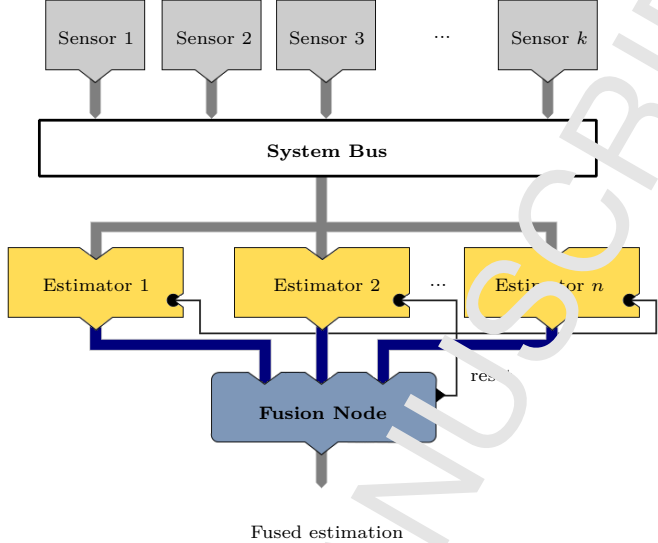


Figure 1: The architecture proposed. Sensor reading processes are enclosed in gray boxes, data is sent through the system bus. Yellow containers encapsulate black-box redundant estimation processes. The blue node corresponds to the fusion algorithm, which weights the contribution from available estimators at a given instant of time. It also fires a reset signal with the available global estimate, so the yellow nodes can be re-initialized.

$$\Psi_{i(t)} = \{\mu_{i(t)}, \Sigma_{i(t)}, \sigma_{i(t)}, \delta t_{i(t)}\}, \quad (1)$$

where  $\mu_{i(t)}$  is the mean state estimate,  $\Sigma_{i(t)}$  is the covariance matrix related to the estimate's error,  $\sigma_{i(t)}$  is the expected deviation of a related neighbor node's estimate from the mean  $\mu_{i(t)}$ , and  $\delta t_{i(t)}$  is the time interval between two successive estimations.

Let an ordering arrangement between nodes  $i \in I$  be established by the fusion node, based on the following assumptions:

**Assumption 1** Nodes  $i \in I$  provide redundant estimates on the system state by encapsulating an estimation process that is unknown to the global fusion policy. Such estimates are assumed to be obtained from nondelayed measurements, and to follow an unimodal distribution, described by a mean value  $\mu_{i(t)}$  and uncertainty covariance matrix  $\Sigma_{i(t)}$ , at time  $t \in \mathbb{R}_{\geq 0}$ .

**Assumption 2** An ordering set of functions  $f_b(i, t)$  describes the reliability of node  $i \in I$ , at time  $t \in \mathbb{R}_{\geq 0}$ , in relation to a behavior profile  $b \in B$ . A total order is established under the relation less than " $\prec$ ", such that the following properties are verified:

- Antisymmetry:

$$\forall b \in B, \forall i, j \in I, t \in \mathbb{R}_{\geq 0}, \\ f_b(i, t) \prec f_b(j, t) \wedge f_b(j, t) \prec f_b(i, t) \Rightarrow i = j.$$

- Transitivity:

$$\forall b \in B, \forall i, j, h \in I, t \in \mathbb{R}_{\geq 0}, \\ f_b(i, t) \prec f_b(j, t) \wedge f_b(j, t) \prec f_b(h, t) \Rightarrow i \prec h.$$

- Totality:

$$\forall b \in B, \forall i, j \in I, t \in \mathbb{R}_{\geq 0}, \\ f_b(i, t) \prec f_b(j, t) \vee f_b(j, t) \prec f_b(i, t) \Rightarrow i \prec j \vee j \prec i.$$

In order to model the previous assumptions, let a set of one-dimensional site arrangements  $S_b \in S$  represent the organization between process nodes  $i \in I$ , under a behavior profile  $b \in B$ . A neighborhood system for  $S_b$  can be defined, such that

$$\mathbb{N}_{b(s)} = \{\mathbb{N}_{bs} | \forall s \in S_b, b \in B\}, \quad (2)$$

where  $\mathbb{N}_{bs}$  is the set of sites neighboring site  $s$ . The sites relationship are subject to the following properties:

- $s \notin \mathbb{N}_s$ , that is, a site is not neighboring to itself.
- $s \in \mathbb{N}_{bg} \Leftrightarrow g \in \mathbb{N}_{bs}$ , that is, a neighboring relationship is mutual.

Let " $\sim$ " be defined by a first-order neighborhood (see Fig. 2), so the clique  $C_s = \{s, w\} | s, w \in S_b$ . Let the left and the right neighbors of a site  $s$  be defined respectively by the functions  $c_{lb}(s)$  and  $c_{rb}(s)$ , such that

$$\begin{aligned} c_{lb}(s) &= g | c_b = \{g, s\}, g \in \aleph_{bs} \\ c_{rb}(s) &= v | c_b = \{s, v\}, v \in \aleph_{bs}. \end{aligned} \quad (3)$$

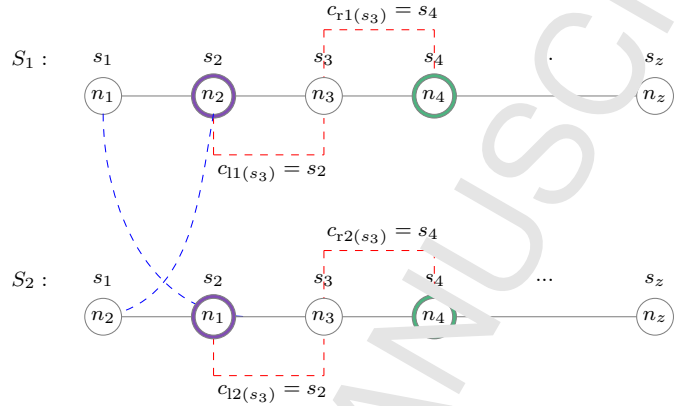


Figure 2: Illustration of one-dimensional first-order neighborhood systems ordering  $z$  process nodes under two distinct behavior profiles. The red dashed paths illustrate cliques conforming to Eq. (3). The blue dashed paths illustrate the change in the placement assigned to nodes  $n_1$  and  $n_2$  in the sites  $S_1$  and  $S_2$ , which are defined considering the distinct behavior profiles.

In the next section it is proposed a neural network structure for modeling the neighborhood arrangements under distinct behavior profiles, and weighting the contribution of the available information from the redundant estimators to the fusion process. As illustrated in Fig. 1, this model would fulfill the functionality described for the Fusion Node.

### 2.1. The neural network B-PR-F

The conceptual feed-forward design of the network proposed is shown in Fig. 3. Let a set of localization task scenarios and conditions (e.g. navigation near the surface, mid-water, seabed, and so on) be represented as individual profiles by the input layer Behavior (Layer B). Hence, the cardinality of the layer is determined from the  $k$  available behavior profiles.

Let the intermediate layer Prediction (Layer P) represent the context anticipation within the neighborhood arrangements, which, as discussed previously,

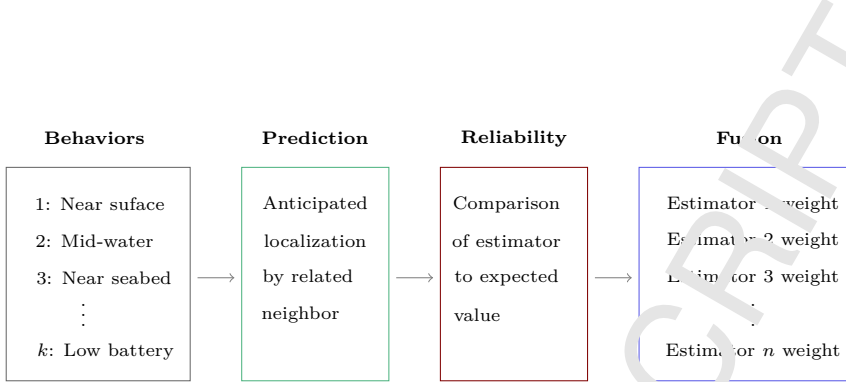


Figure 3: The Neural Network design principle.

are specific to each behavior profile. Consequently, neurons at this layer encode the parameter  $\sigma_{i(t)}$  in standard deviation units (see Eq. (1)), which represents the delimitation of the expected deviation from the region surrounding  $\mu_{i(t)}$ , within which the estimate by the related neighbors to process  $i$  should fall. Therefore, the activation of the layer's neurons is expected to become stronger as the task progresses, since uncertainty is expected to increase with robot motions and time pass.

Let the intermediate layer Reliability (Layer R) encode the confidence on the nodes' estimate in relation to the predicted value. Thus, once a node passes the test with a certain probability, the related unit in Layer P is reinitialized. The cardinality of both intermediate layers (P and R) is determined from the  $k$  number of behavior profiles, and the  $n$  number of available estimators.

Let the output layer Fusion (F) represent the fusion weight assigned to the information provided by each estimator node available, at a given instant of time. Hence, the cardinality of the layer is determined from the  $n$  number of estimators available in the system. From the activation of the layer, the global estimate is calculated by the weighted sum of the estimators' output. The structure of the neural network designed is shown in Fig. 4. Due to the result feed forward layered architecture, the network is named B-PR-F. Next, a proposal for the model implementation is detailed.

*Network parameters.* Let the weight matrix  $\mathbf{W}_{[k \times kn]}^{\text{BP}}$  condition the activity of the intermediate layers to the local neighborhoods, according to the selected

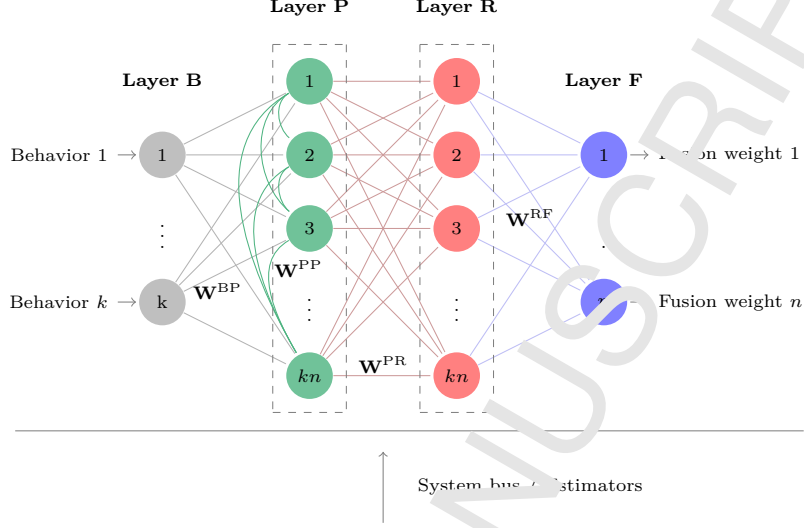


Figure 4: The B-PR-F Neural Network for data fusion. The circles represent neurons in each layer, and the edges illustrate the connectivity between layers. The intermediate layers are shown within the dashed central region. The cardinality of the intermediate layers is determined from the  $k$  number of behavior profiles, and the  $n$  number of available estimators. The weight matrices interconnecting the neuron layers are denoted by  $\mathbf{W}^{BP}$ ,  $\mathbf{W}^{PR}$ , and  $\mathbf{W}^{RF}$ . The lateral connections  $\mathbf{W}^{PP}$  model changes in the activation of layer P due to behavior profile transitions

behavior profile. Therefore, it is set as the multiplexed identity matrix, such that

$$\mathbf{W}^{BP} = \begin{bmatrix} \mathbf{1}_{[1 \times n]} & \cdots & \mathbf{0}_{[1 \times n]} \\ \vdots & \ddots & \vdots \\ \mathbf{0}_{[1 \times n]} & \cdots & \mathbf{1}_{[1 \times n]} \end{bmatrix}. \quad (4)$$

Let the matrix  $\mathbf{W}^{PP}_{[kn \times kn]}$  represent the lateral connections of Layer P, so changes in the activation of layer P due to behavior profile transitions can be modeled. In case no interaction between behavior profiles would be desired  $\mathbf{W}^{PP}_{[kn \times kn]} = \mathbf{I}_{[kn]}$  is set to the identity, otherwise  $\mathbf{W}^{PP}_{[kn \times kn]} = f(t, \Psi_{(t)})$ , with  $f(t, \Psi_{(t)})$  an arbitrary function depending on time  $t$ , defined according to the characteristics of the task and the estimators' parameters  $\Psi_{(t)}$  (see Eq. (1)).

Let the matrix  $\mathbf{W}^{\text{PR}}_{[kn \times kn]}$  represent the connectivity within the node neighborhoods, and be given by

$$\mathbf{W}^{\text{PR}} = \begin{bmatrix} \mathbf{W}^1 & \cdots & -\varsigma \mathbf{I}_{[n]} \\ \vdots & \ddots & \vdots \\ -\varsigma \mathbf{I}_{[n]} & \cdots & \mathbf{W}^k \end{bmatrix}. \quad (5)$$

where  $\varsigma$  corresponds to a high magnitude weight assigned to unrelated neighbors (i.e. the inhibition of neighborhood arrangements that are related to other behavior profiles). Let the matrices  $\mathbf{W}^y | y \in \{1, 2, \dots, k\}$ , in the diagonal section be obtained from the system configuration matrix  $\mathbf{W}^N_{[kn \times n]}$ , which is provided by the system designer, and represents knowledge on the estimators' reliability along each behavior profile. Hence,  $\mathbf{W}^y$  encodes the ordered arrangements of nodes according to the behavior profiles. It can be modeled analytically by fixing stronger weights to first-order clique excitatory weights to left neighbors, and inhibitory weights to right neighbors, such that

$$\mathbf{W}_{ij}^y = \begin{cases} (\mathbf{W}_{yi}^N - \mathbf{W}_{yj}^N)^{-1} & \text{if } i \neq j \\ 0 & \text{otherwise} \end{cases}. \quad (6)$$

Let the matrix  $\mathbf{W}^{\text{RF}}_{[k, \times n]}$  be obtained from the rows of  $\mathbf{W}^N$ , such that

$$\mathbf{W}^{\text{RF}} = \begin{bmatrix} \text{diag}(\mathbf{W}_{1:}^N) \\ \vdots \\ \text{diag}(\mathbf{W}_{k:}^N) \end{bmatrix}. \quad (7)$$

Let the clique functions  $c_{lb}(i)$  and  $c_{rb}(i)$ , which allow to query respectively the left and right neighbor of a given node  $i$  (see Eq. (3)), be defined in the network structure such that

$$\begin{aligned} \check{c}_l(i) &= \arg \max_{q=1, \dots, kn} \mathbf{W}_{iq}^{\text{PR}} \\ \check{c}_r(i) &= \arg \max_{j=1, \dots, kn} \mathbf{W}_{ji}^{\text{PR}} \end{aligned} . \quad (8)$$

Finally, let the correspondence between the sites represented in the intermediate layers (P and R) and the estimator nodes available in the system be established through the mapping function  $m(\cdot)$ , which is defined such that

$$m(i) = \min_{j \in 1, \dots, n} (\text{mod}(i, j)) , \quad (9)$$

where  $\text{mod}(\cdot, \cdot)$  is the modulus function.

*Layers' activation.* Let the activation of layer B be defined according to the winner-takes-all policy (i.e. only one behavior is expected to be active at a time), applied to an arbitrary function  $f(j, t)$ , such that

$$\mathbf{b}_{i(t)} = \begin{cases} 1 & \text{if } i = \arg \max_{b \in B} f(b, t) \\ 0 & \text{otherwise} \end{cases} . \quad (10)$$

Let the activation of neurons in Layer P be defined by

$$\mathbf{p}_{i(t)} = \sum_j \mathbf{W}_{ij}^{\text{BP}} \mathbf{b}_{j(t)} \cdot \max \left( \kappa(\mathbf{r}_{(t-1)}, i) \sum_g \mathbf{W}_{ig}^{\text{PP}} \mathbf{p}_{g(t-1)} + \frac{\delta t}{\tau_i}, 1 \right) \quad (11)$$

where  $\kappa(\mathbf{r}_{(t-1)}, i) = h(\mathbf{r}_{d(t-1)})|d = r(i)$  (see Eq. (8)) is a reset function considering the reliability test applied to the right neighbor of the  $i^{\text{th}}$  unit (as encoded by Layer R),  $h(\cdot)$  is the Heaviside step function,  $\delta t$  is the time change, and  $\tau_i$  is an heuristic parameter representing a time scaling factor.

Let the information represented in Layer R be determined based on the parameters provided by left neighbors in the ordered arrangements. Hence, the parameter set  $\psi_{(t)} = \{\Psi_{1(t)}, \dots, \Psi_{n(t)}\}$  (see Eq. (1)) is conceptually selected such that

$$\psi_{(t)} = \begin{cases} \Psi_j & \text{if } \exists j | j = c_{lb}(i) \\ \Psi_i & \text{otherwise} \end{cases} . \quad (12)$$

For the network implementation proposed, let  $\hat{\psi}_{(t)} = \{\hat{\mu}_{(t)}, \hat{\Sigma}_{(t)}, \hat{\sigma}_{(t)}, \hat{\delta t}_{(t)}\}$  be selected by relying on Eqs. (8) and (9), thus

$$\hat{\psi}_{(t)} = \Psi_j | j = m(\check{c}_l(i)). \quad (13)$$

Let the activation of Layer R be defined by

$$\mathbf{r}_{i(t)} = \mathbf{a}_{i(t)} h(\gamma_i(t) - \phi_1) \gamma_i(t), \quad (14)$$

where  $\mathbf{a}_{[nk]}$  is a binary column vector indicating the availability of new estimations at a given instant of time. It is defined by concatenating  $k$  times the boolean values for  $n$  estimator nodes. The parameter  $\phi_1$  represents a threshold value applied in the reliability test. The function  $\gamma_i(t)$  is defined, such that

$$\gamma_i(t) = \frac{1}{1 + \exp(-\phi_2(\hat{\sigma}_{(t)} - \beta_i(t)))}, \quad (15)$$

where  $\hat{\sigma}_{(t)}$  determines the sigmoid midpoint and the parameter  $\phi_2$  modulates the steepness of the curve. The function  $\beta_i(t)$  is defined by

$$\beta_i(t) = \mathbf{x}_{i(t)}^\top \mathbf{V}_{i(t)}^{-1} \mathbf{G}_{i(t)}^{-1} \mathbf{V}_{i(t)} \mathbf{x}_{i(t)}, \quad (16)$$

with  $\mathbf{x}_{i(t)} = \mu_{i(t)} - \hat{\mu}_{(t)}$ . The matrix  $\mathbf{V}_{i(t)}$  corresponds to the  $\hat{\Sigma}_{(t)}$  eigenvectors, and  $\mathbf{G}_{i(t)} = \hat{\sigma}_{(t)} \text{diag}(\lambda_{(t)})$  is defined from its eigenvalues  $\lambda_{(t)}$ .

Let the activation of Layer F be given by

$$\mathbf{f}_{(t)} = \|\mathbf{W}^{\text{RF}} \mathbf{r}_{(t)}\|_1. \quad (17)$$

Finally, let the fused system parameters estimation  $\bar{\mu}_{(t)}$  and  $\bar{\Sigma}_{(t)}$  be obtained by weighting all  $n$  estimators' output proportionally to the activation of Layer F, thereby

$$\begin{aligned} \bar{\mu}_{(t)} &= \mathbf{f}_{(t)}^\top [\mu_{1(t)} \cdots \mu_{n(t)}]^\top \\ \bar{\Sigma}_{(t)} &= [\mathbf{f}_{1(t)} \mathbf{I}_{[d]} \cdots \mathbf{f}_{n(t)} \mathbf{I}_{[d]}] [\Sigma_{1(t)} \cdots \Sigma_{n(t)}]^\top, \end{aligned} \quad (18)$$

where  $\mathbf{I}_{[d]}$  is the identity matrix, with  $d$  the dimension of the task state space.

### 3. Materials and methods

The simulation study was conducted in the Gazebo Robot Simulator version 7.0 (see Fig. 5). The scenario considered was *oceans-waves* by Manhães et al. [18], running in the Robot Operative System (ROS) version Kinetic Kame. The dataset was generated by defining a way-points trajectory, so the robot attempted to pass near the points while interacting with the particle physics engine, which models dynamics from the aquatic medium. The data generated was processed in GNU Octave version 4.0.0, so the performance of the network was analyzed under two distinct navigation conditions. All the software used in the study run on the Ubuntu operative system, version 16.04.

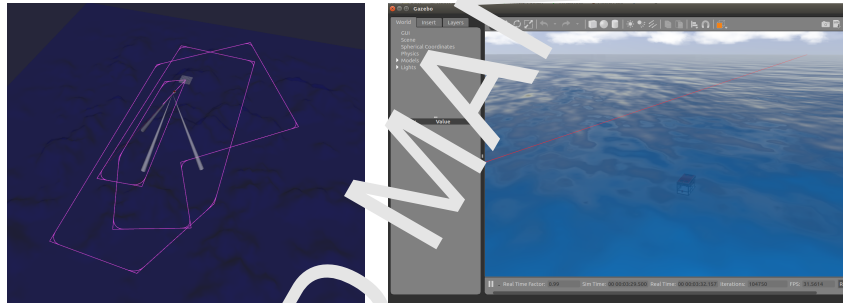


Figure 5: The simulation environment. On the left, the visualization generated by the RViz node, running in ROS Kinetic Kame (under Ubuntu version 16.04). It is shown the trajectory executed by the virtual robot in the *JUV-Simulator* (Unmanned Underwater Vehicle - UUV). On the right, the view of the *oceans-waves* scenario by Manhães et al. [18], running on the robot simulation software Gazebo version 7.0.

The experiment was performed in a harbor area of the Yacht Club of Rio Grande, Fazil, with a ROV Seabotix<sup>©</sup> LBV300-5, equipped with an on-board compass, a Teledyne Blueview<sup>©</sup> Forward-Looking SONAR P900-130, a Tritech<sup>©</sup> MicroNav UCBL system, and a SOUTH<sup>©</sup> S82T DGPS. The trajectory of the ROV was controlled by a human operator. Thanks to a stand-up board fixed on the vehicle (see Fig. 6), the DGPS portable controller remained over the water surface while the vehicle remained underwater, in a constant depth of 0.7 meters, and approximated 3 meters from the seabed during the experiment.

The dataset was processed off-line, so the implemented algorithms are compared based on GNU Octave version 4.0.0 implementations<sup>2</sup>. Both the simulation and experimental task environment and results can be visualized on-line<sup>3</sup>.

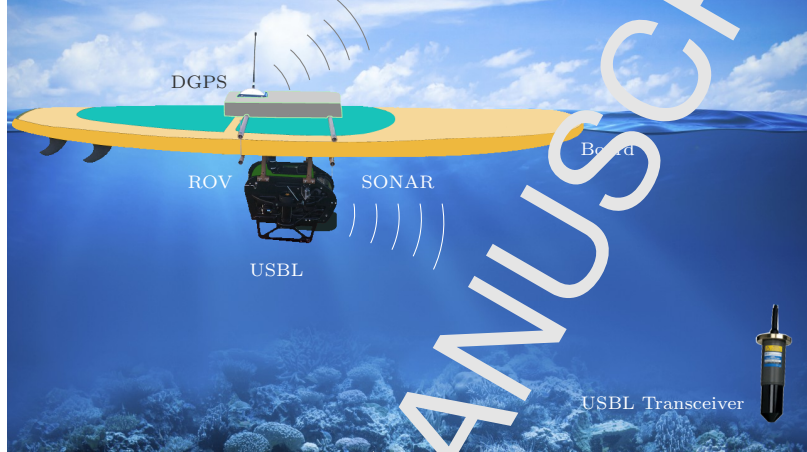


Figure 6: The robot Seabotix attached to a surfboard.

#### 4. Simulation

In order to study the performance of the model, a localization task involving two behavior profiles was designed in simulation. The situation depicted consisted in an exploration mission where the ROV is launched from a fixed operation base to navigate shallow and deep water. Once the predefined trajectory is completed, the vehicle would return to the launch point to be collected.

The first behavior profile designed consists in navigating near the surface. In this situation on board estimation of motion could rely on inertial sensory, as for example, on the *inertial measurement unit* (IMU), which provides estimates on the linear accelerations and the rotational rate of the vehicle. For global positioning axes, the robot would count on the USBL and the DGPS sensors,

---

<sup>2</sup> The sources can be downloaded from: <https://github.com/henferch/B-PR-F>  
<sup>3</sup> An illustrative video is available at: <https://youtu.be/a0PSj8vMPnM>

although measures from the later would be available only when surfacing (since the GPS radio frequency is hardly received in the underwater medium). The second behavior profile corresponds to navigating close to the seabed. In this case the on-board motion estimation could rely on more sophisticated sensory, such as the *Doppler velocity log* (DVL) sensor, which propagates an acoustic wave to the seabed, producing an estimate of the vehicle's velocity. Under this profile global fixes would be received only from the USBL sensor. Table 1 summarizes the scenarios described. The obtained results are reported next.

Condition	Description
Near surface	DVL measurements are noisy in deep water, notably, when the vehicle is too far away from the seabed. Sensory reliability: DVL ≺ IMU ≺ USBL ≺ DGPS
Near seabed	The DVL sensor is able to provide useful estimates since the acoustic signal can be propagated to the seabed. Sensory reliability: DGPS ≺ IMU ≺ DVL ≺ USBL

Table 1: Navigation conditions considered in the simulated scenario.

#### 4.1. Simulation results

As shown in Fig. 4, the fusion architecture included information provided by four estimators. The first two estimators would encapsulate computational processes that estimate the vehicle's localization based on dead reckoning (DR). Conforming to the behavior profiles defined in Table 1, by relying on the IMU, E1 is expected to be more precise when the vehicle is near the surface, whereas, by relying on the DVL, E2 would produce better results when the vehicle is near the seabed. The estimators E3 and E4 would encapsulate positioning system (PS) measurements, respectively, from the USBL and the DGPS sensors. The altimeter (ALT) would provide estimates on the distance from the seabed, this information is considered to switch between the two behavior profiles described. Figure 8 shows the resulting B-PR-F neural network implemented.

In Appendix A detailed information about the simulation parameters and the model is provided.

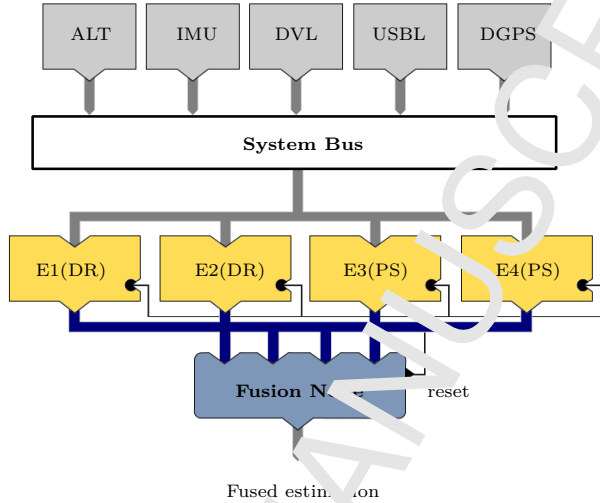


Figure 7: Fusion architecture for the simulation study.

In real underwater scenarios the USBL measurements are affected by noise following a Gaussian distribution. Moreover, the noise variance is expected to increase as the distance between the vehicle and the fixed transceiver location increases. Non-Gaussian noise is also expected to affect the USBL measurements, this would correspond to random physical interference on the transmission of the acoustic signals. The previous assumptions were simulated in the study (see Appendix A). Figure 9 illustrates a comparison on the root-mean-square (RMS) error of the vehicle localization estimates issued by the model, and the USBL readings when they were available. As noted, the B-PR-F neural network is able to filter out the non-Gaussian noisy readings from the virtual USBL sensor.

Figure 10 presents the 3D visualization of the localization estimation by the B-PR-F model, compared to the ground truth and to the USBL data. The path followed under the first behavior profile (i.e. navigating near the surface) is plotted in blue, whereas the path followed under the second behavior profile (i.e. navigating near the seabed) is shown in red. Figure 11 presents the accumulated

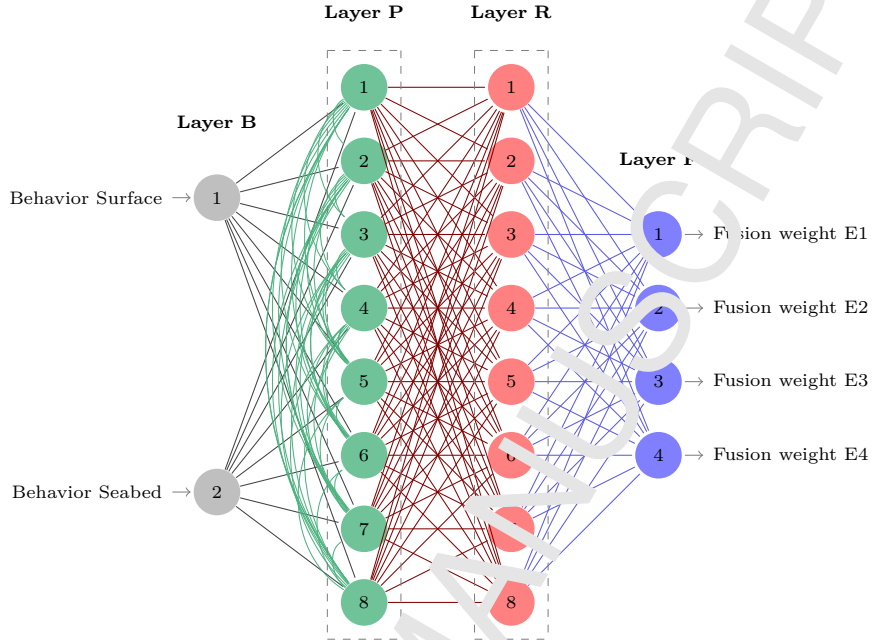


Figure 8: The B-PR-F neural network implemented for the simulation study.

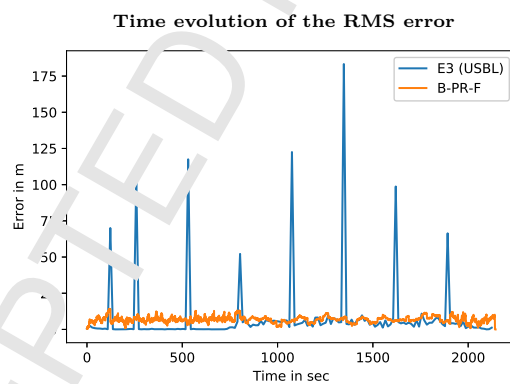


Figure 9: Comparison on the B-PR-F model estimates and the noisy USBL readings, with respect to the ground truth.

RMS error, obtained by using only one or the two behavior profiles modeled. As noted, the estimates resulting from the fusion of information provided by the two behavior profiles presented the best results.

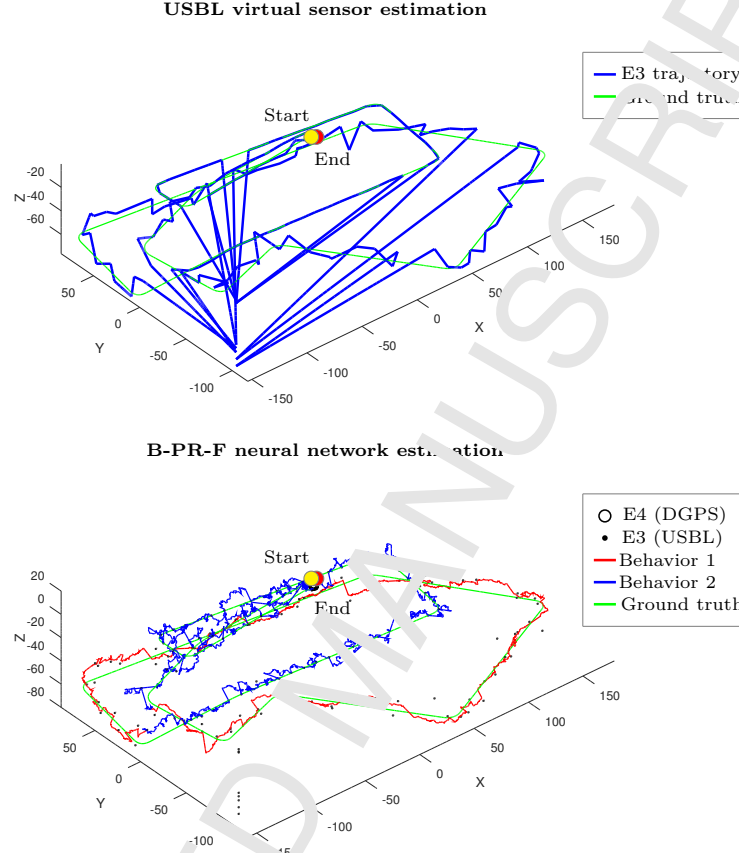


Figure 10: Comparison on the B-PR-F model performance to the USBL sensor simulation. The initial and final locations of the vehicle are shown by the big circles.

The principle of contextual anticipation of information within ordered neighborhoods is illustrated in Fig. 12, where a segment of the simulation is shown, under the activation of the behavior profile 2. In the figure only the XY Cartesian coordinates are plotted for visualization clarity. The boundary of the anticipated region  $r = \mathbf{p}_{6(t)}\Sigma_{2(t)}$  is represented from the covariance matrix  $\Sigma_{2(t)}$  (associated to E2's estimation error) and the activation of the 6<sup>th</sup> unit of Layer 1 (see Eq. (11)), which encodes the expected deviation of E3's estimates with respect to E2's estimates.

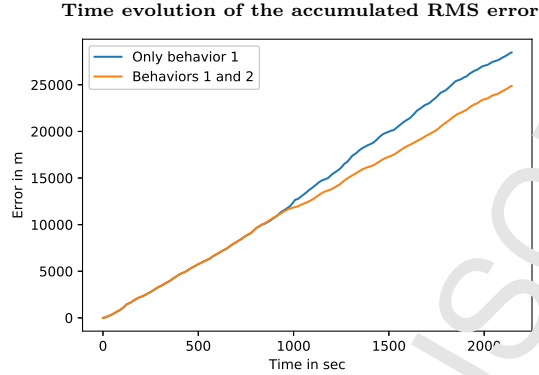


Figure 11: Comparison on the accumulated RMS error. As expected, the fusion of multiple behavior profiles produced better results, given the distinct scenarios modeled in the task.

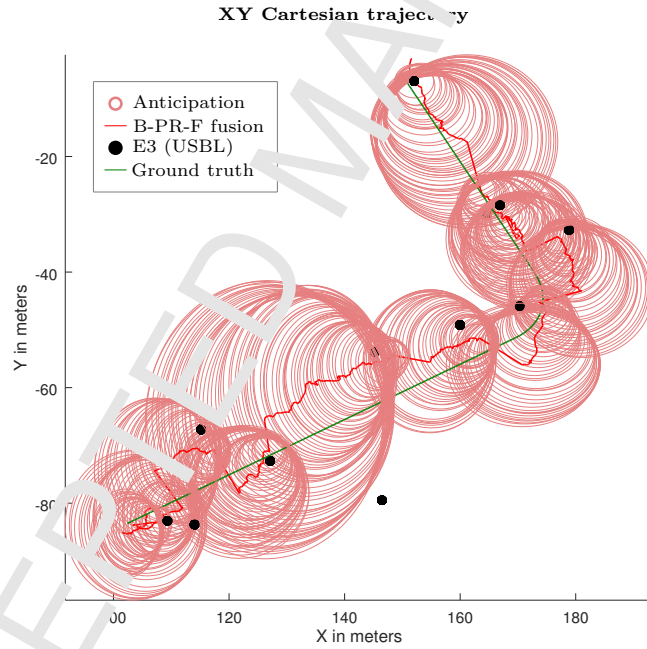


Figure 12: Visualization of the principle of information anticipation.

Figure 13 presents the evolution of the activation of the layer units for the trajectory illustrated in Fig. 12. It can be noticed that the B-PR-F neural net-

work proceeded to the fusion of information when the reliability of the predicted signal ( $E_3$ ) fell within the acceptance region, anticipated by the predictor node ( $E_2$ ). In such a case, the network issued a reset signal to the corresponding unit in Layer P. Thereby, Layer P represents a measure on the precision of the anticipation in standard deviation units. This information can be valuable for the detection of abnormal situations (e.g. unexpectedly large values in  $p_{6(t)}$  may suggest malfunction of the node  $E_3$ ). Consequently from the neighborhood arrangement heuristics and the evaluation of information encoded by the network, the fusion weights assigned by the activation of Layer F were able to reject unexpected disturbances, showing robustness to unmodeled noise.

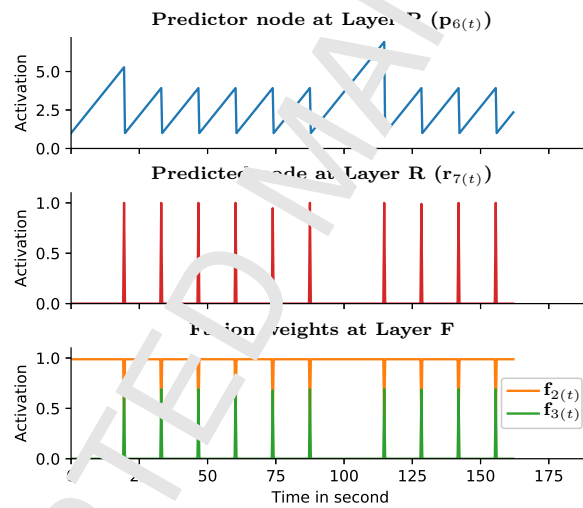


Figure 13: Activation of units relevant to the trajectory shown in Fig. 12, under the behavior profile 2. The plot illustrates the B-PR-F principle of reliable fusion of information and reset.

In order to study the role of the lateral connections modeled in Layer P, the matrix  $\mathbf{V}^{PP}$  was set according to two different conditions. In the first scenario  $\mathbf{W}^{PP} = \mathbf{I}_{[kn]}$  was set to the identity. Thus, it would correspond to the condition of no interaction between the predictions performed under the behavior profiles. The second condition was designed to analyze whether the

information gathered within one behavior profile could be useful for the other profile. Thereby, interaction was modeled such that

$$\mathbf{W}^{\text{PP}} = \begin{bmatrix} I_{[n]} & f(S_1, S_2) & \cdots & f(S_1, S_b) \\ \vdots & \vdots & \ddots & \vdots \\ f(S_b, S_1) & f(S_b, S_2) & \cdots & I_{[n]} \end{bmatrix} \quad (19)$$

with the function  $f(S_a, S_z)$  defining the sparse encoding matrix, that maps the activation of units representing left neighbors in  $S_a$ , to units representing left neighbors in  $S_z$ . The correspondence mapping  $m(S_a, S_z)$  from profile  $a$  to profile  $z$  is obtained by applying Eq. (8), thus

$$m(S_a, S_z) = c_{lz} \quad \forall a \in S_a, \forall z \in S_z. \quad (20)$$

Figure 14 presents a comparison on the two conditions described above. As noted, although it was not always the case, the fact of allowing interaction between the behavior profile predictions tended to produce overall positive effects over the estimates.

## 5. Experimental

The experimental task is illustrated in Fig. 15. The vehicle traveled approximately 693 meters in 61 minutes. The SONAR tilt was about  $0^\circ$  regarding the horizon, its field of view covered a horizontal opening of  $130^\circ$  and a range of 50 meters. In total, it was recorded 19992 grayscale 16-bits images by the SONAR, 2563 heading values by the compass, 3662 positions by the DGPS, and 1450 positions by the USBL.

### 5.1. The localization task

The ground truth measurements available corresponded to the geo-referenced Cartesian coordinates of the robot, as registered by the DGPS. Thus, the state representation of the task is such that

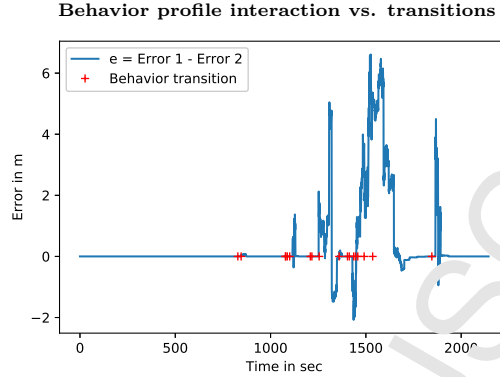


Figure 14: Comparison on the relative RMS error for the constraint "Error 1" ( $\mathbf{W}^{PP} = \mathbf{I}_{[kn]}$ ), and "Error 2" ( $\mathbf{W}^{PP}$  set conforming to Eq. (19)). In the comparison, behavior change was enforced by setting a lower threshold of 20 m to the ultrameter measurement (which is different from the value set in the simulation shown in Fig. 10, that considered a 30 m threshold). This is done so more transitions between the profiles were produced, as the robot navigated near the seabed.

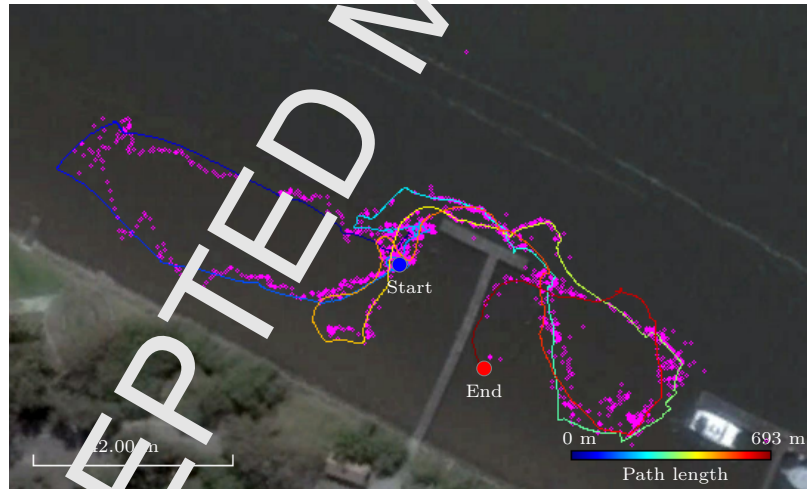


Figure 15: The traveled path of the vehicle recorded by the DGPS starting with blue line color and ending with red line color. The magenta dots represent the USBL measurements. Map data: Google<sup>©</sup>, DigitalGlobe<sup>©</sup> 09-29-2016, 32° 1' 29.9568" S 52° 6' 24.6096" W. The initial and final locations of the ROV are shown by the big circles.

$$\mathbf{x} = [x \ y]^\top. \quad (21)$$

Only one behavior profile (i.e. navigation near the surface) was considered due to the experimental setup. Two redundant estimators were implemented. The first one relied entirely on dead reckoning. The second one consisted in a KF algorithm, which included dead reckoning information in the predictive step, and USBL measurements in the correction step. Nevertheless, the implementation details of these estimators are provided.

*Scan-matching motion estimation.* The relative motion of the vehicle is estimated from the information provided by the multi-beam SONAR sensor. Differently from mechanical devices (see Burgos et al. [19]), the sensor captures the acoustic beams at once, making it possible in both stationary and moving platforms, and avoiding the need for introducing corrections due to motion. The Lucas-Kanade method (Lucas & Kanade [20]) implemented in OpenCV version 3.3 was used to perform the scan-matching. The relative change in the robot instantaneous posture between two consecutive acquisitions is estimated from  $w$  matching points, by solving the overdetermined system of the form

$$\rho = ([\mathbf{A}_1 \cdots \mathbf{A}_w]^\top)^+ [\mathbf{b}_1 \cdots \mathbf{b}_w]^\top \quad (22)$$

where  $(\cdot)^+$  denotes the Moore-Penrose inverse, and

$$\begin{aligned} \mathbf{A}_i &= \begin{bmatrix} \cos(\Delta\theta) & \sin(\Delta\theta) & \Delta x & \Delta y \end{bmatrix}^\top, \\ \mathbf{A}_i &= \begin{bmatrix} x_{i(t-1)} & y_{i(t-1)} & 1 & 0 \\ y_{i(t-1)} & x_{i(t-1)} & 0 & 1 \end{bmatrix}^\top, \\ \mathbf{b}_i &= \begin{bmatrix} x_{i(t)} & y_{i(t)} \end{bmatrix}. \end{aligned} \quad (23)$$

The parameters of interest are the 2D pose of the ROV. That is, the Cartesian displacement  $\Delta x$ ,  $\Delta y$ , and the yaw orientation  $\Delta\theta$ , obtained from  $\rho$ . The dead reckoning estimation is obtained by integrating the relative displacements of the robot over time.

*Kalman Filter estimation.* A classical KF (Thrun et al. [9]) was implemented. The estimated state vector  $\mathbf{x}_{(t)}$  is such that

$$\mathbf{x}_{(t)} = \mathbf{F}_{(t)}\mathbf{x}_{(t-1)} + \mathbf{B}_{(t)}\mathbf{u}_{(t)} + \epsilon_{(t)}, \quad (24)$$

where  $\mathbf{F}_{(t)}$  is the state transition model,  $\mathbf{B}_{(t)}$  in the control input model,  $\mathbf{u}_{(t)}$  is the control vector input, and  $\epsilon_{(t)}$  is a random Gaussian vector that models the uncertainties introduced by the state transition. The predicted state estimate and covariance are

$$\begin{aligned} \tilde{\mathbf{x}}_{(t|t-1)} &= \mathbf{F}_{(t)}\tilde{\mathbf{x}}_{(t-1|t-1)} + \mathbf{B}_{(t)}\mathbf{u}_{(t)} \\ \tilde{\mathbf{P}}_{(t|t-1)} &= \mathbf{F}_{(t)}\tilde{\mathbf{P}}_{(t-1|t-1)}\mathbf{F}_{(t)}^\top + \mathbf{Q}_{(t)}. \end{aligned} \quad (25)$$

The a posteriori state correction is given by

$$\begin{aligned} \hat{\mathbf{x}}_{(t|t)} &= \tilde{\mathbf{x}}_{(t|t-1)} + \mathbf{K}_{(t)}\tilde{\mathbf{y}}_{(t)} \\ \hat{\mathbf{P}}_{(t|t)} &= (\mathbf{I} - \mathbf{K}_{(t)}\tilde{\mathbf{H}}_{(t)})\tilde{\mathbf{P}}_{(t|t-1)} \\ \tilde{\mathbf{y}}_{(t)} &= \mathbf{z}_{(t)} - \tilde{\mathbf{H}}_{(t)}\tilde{\mathbf{x}}_{(t|t-1)} \\ \mathbf{S}_{(t)} &= \mathbf{R}_{(t)} + \mathbf{H}_{(t)}\mathbf{P}_{(t|t-1)}\mathbf{H}_{(t)}^\top \\ \mathbf{K}_{(t)} &= \mathbf{P}_{(t|t-1)}\mathbf{H}_{(t)}^\top \mathbf{S}_{(t)}^{-1} \end{aligned}, \quad (26)$$

where  $\mathbf{H}_{(t)}$  is the observation matrix.

Other matrices are set to:  $\mathbf{Q}_{(t)} = \text{diag}(\sigma_{\text{odom}})$ ,  $\mathbf{R}_{(t)} = \text{diag}(\sigma_{\text{usbl}})$ ,  $\mathbf{F}_{(t)} = \mathbf{B}_{(t)} = \mathbf{H}_{(t)} = \mathbf{I}$ . Data related to the intended motion of the robot was not available, thus, the intent  $\mathbf{u}_{(t)}$  was taken as the dead reckoning estimate, which is obtained by integrating the estimation of the relative displacement of the robot (from the SOTAP scan-matching) along the motion direction, as estimated by the compass sensor. Measurements  $\mathbf{z}_{(t)}$  are acquired from the USBL sensor.

## 6. Results

The fusion architecture implemented for the experimental task is illustrated at the top of Fig. 16. On the bottom of the figure it is shown the structure of the learning B-PR-F neural network. The model was implemented conforming to parameters set detailed in Appendix B.

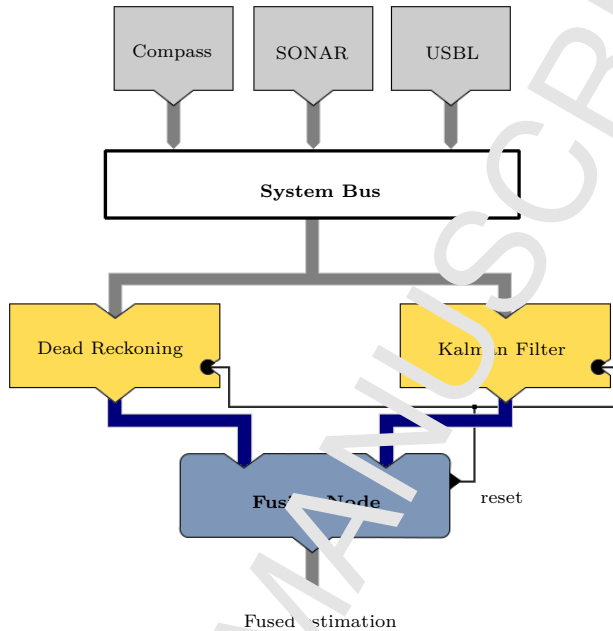
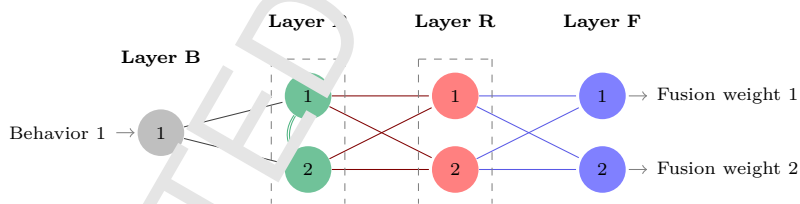
*Experimental Architecture**Fusion Node: Neural Network B-PR-F*

Figure 16: Architecture for the experimental study. Given the characteristics of the task, a single behavior profile was modeled in Layer B (navigating near the surface). The estimator nodes available were dead reckoning and the Kalman Filter.

Figure 17 shows the results obtained from the scan-matching algorithm. Figure 18 presents the estimates by the network compared to: a) dead reckoning, b) the KF algorithm, and c) the Augmented MCL (A-MCL) particle filter algorithm (Thrun et al. [9]), that is robust to the robot kidnapped problem. The ground truth (DGPS) and the USBL estimates are also shown. Figure 19

illustrates the aspect of context anticipation from the information represented in Layer P. As it can be noticed, the B-PR-F network was able to restrict unmodeled noise to the anticipated green regions, which produce estimates more close to the ground truth.

In order to compare the performance between the algorithms in a close to Gaussian error distribution scenario, data was post-processed to remove potentially invalid USBL measurements, and given to the 'KF implementation. Table 2 presents the RMS error, the standard deviation, and the average processing time in sec. The accumulated error in the experiment is shown in Fig. 20.

Algorithm	Mean	Sta. Dev.	Time
Dead reckoning	45.7770	20.9248	<b>0.3179</b>
Kalman Filter	1.9479	3.0804	0.3227
A-MCL	1.5963	1.2146	5.0440
Kalman Filter Post-processed	1.4378	1.6161	0.3215
B-PR-F Neural Network	<b>1.4139</b>	<b>1.1479</b>	0.6302

Table 2: Algorithms evaluation. The comparison is done by running off-line the captured data, in GNU Octave version 4.0.0 implementations of the algorithms. The RMS localization error is expressed in m, and the mean processing time per iteration is indicated in sec. The Kalman Filter Post-processed estimator is obtained by previously excluding USBL measures relative to the transceiver's location from the dataset.

## 7. Discussion

The study conducted in the virtual environment illustrated the usefulness of the B-FR-N neural network in representing the local arrangements between estimators (see Figs. 10 and 11), as related to particular scenarios encountered in the underwater localization task. The results obtained pointed out the relevance of contextual anticipation of information for obtaining a more informed and reliable fusion. This principle has been explored in a previous research for humanoid robotics localization (Chame & Chevallerau [17]) and could be successfully extended to the field of underwater robotics localization.

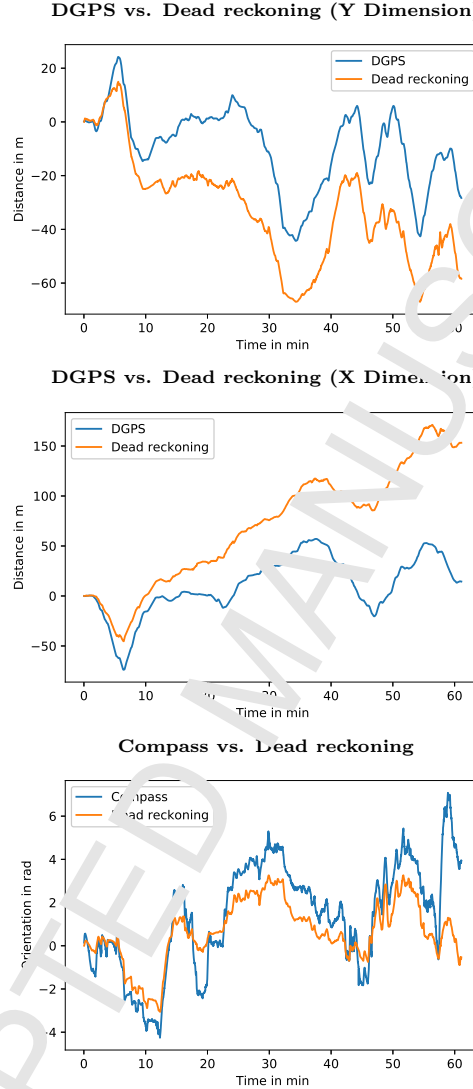


Figure 17: Comparison between the scan-matching dead reckoning estimates and the reference values from the DGPS and the compass sensors, in the linear  $x$  and  $y$ , and the angular  $\theta$  dimension. The obtained correlations were  $c_x = 0.8142$ , and  $c_y = 0.8832$ ,  $c_\theta = 0.8766$ .

The design of the B-PR-F network structure also extended our previous work in which the model BAR-F (for Behavior, Activation, Reliability and Fusion) was proposed (see Chame et al. [21]). Although these two models can be consid-

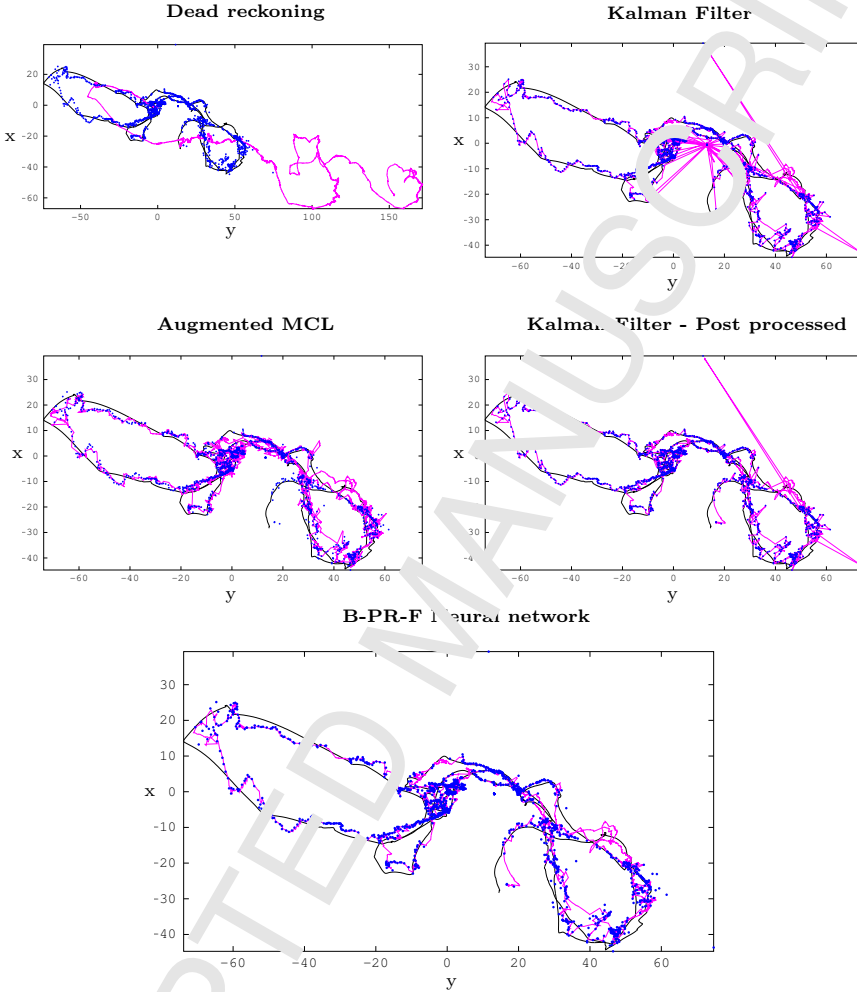


Figure 18: Trajectory visualization. The estimation is shown in magenta, the ground truth is shown in black, and the USBL measurements are shown as blue dots.

ered to produce equivalent results in several aspects, there are two advantages of B-PR-F with respect to its predecessor. The first advantage is the fact of representing information related to the contextual anticipation explicitly in Layer P. As it was suggested in the simulation study (see Figs. 12 and 13), this can be a valuable resource to analyze the performance of the system at a given instant

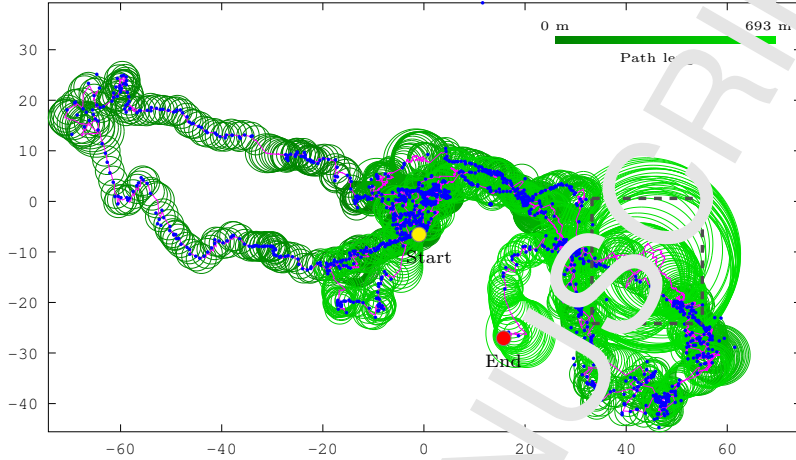


Figure 19: Trajectory visualization with anticipation. Distances are expressed in meters. The predicted region by Layer P is shown in green, the B-PR-F fusion is shown in magenta, and the USBL data is shown as blue dots. The dashed box points out to a momentary increase of uncertainty, due to disturbances affecting the USBL measurements. The initial and final locations of the ROV are shown by the circles.

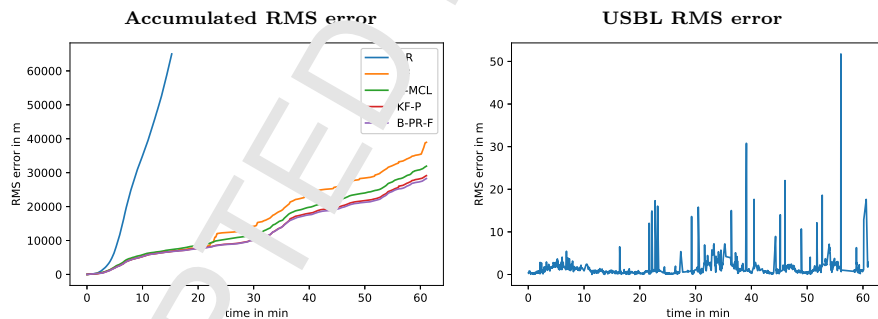


Figure 20: On the left the visualization of the accumulated RMS estimation errors, relative to the ground truth, for the algorithms: dead reckoning (DR), A-MCL, Kalman Filter (KF), KF with deep post-processing, and the neural network B-PR-F. As noticed, B-PR-F presented the lowest accumulated error (which is also described in Table 2). On the right it is shown the USBL localization error. As observed, errors do not accumulate in the USBL sensor estimation, but measurements are affected by non-Gaussian noise.

of time, and detecting sensory performance degradation. We believe that this information can be relevant to the selection arbitration function for changing to a different operation estimation mode or behavior. This aspect will be explored in future research. The second advantage is the possibility of modeling behavior profile interactions through the lateral connections of matrix  $\mathbf{W}^{PP}$ , as illustrated in Fig. 14. Nonetheless, there is a disadvantage of B-PR-F in relation to BAR-F that should be mentioned, which is the fact of being computationally less efficient, since the cardinality of the hidden layers increases proportionally to  $kn$  (with  $k$  behavior profiles and  $n$  number of estimators available), and not to  $n$  (the BAR-F network does not have hidden layers).

Regarding the experimental study the scan-matching algorithm provided interesting results. In this sense, measurements were highly correlated to the reference values (see Fig. 17). As expected, however, the trajectory obtained by dead reckoning drifted over time (see Table 2), which indicates the relevance of introducing global position corrections to the estimates. This aspect has been addressed in the literature (e.g. in Drolet et al. [5]). Some important factors that contribute to the imprecisions in the underwater medium are: a) the absence of features in the scene, or, to be more specific, in the acoustic images (e.g. the robot is navigating near the surface in deep water), and b) the presence of dynamic features (e.g. fishes swimming around), which are independent from the robot motion.

The KF algorithm considered fixes from the USBL sensor, though estimates were severely affected by non-Gaussian noise. This can be particularly observed when the USBL sensor was not able to provide a reliable measurement, and simply returned the relative coordinates of the transceiver. The problem was mitigated by heuristically ignoring such measures. Nevertheless, as shown in Fig. 18, estimates were still affected by unmodeled noise.

As a multi-modal distribution estimation, A-MCL was able to handle noise, running with an 1000-particles population (see Fig. 18). The B-PR-F network was also able to handle noise, but at a much lower computational cost. In this sense, the fusion heuristic based on the contextual anticipation of the neighbor's

signal, was able to conveniently take advantage on available unimodal state estimations. Although the resultant fusion process is formally of quadratic order  $O((nk)^2)$ , due to the intermediate layers matrix multiplications (with  $n$  estimators and  $k$  behavior profiles); given the structure of the weight matrices, it is possible to obtain more efficient implementations. Another advantage of the B-PR-F network over A-MCL is the fact that the former is a deterministic algorithm, whereas the later is not. Indeed, A-MCL presented occasionally degraded performance, since particles are randomly generated.

When analyzing the average execution time per iteration shown in Table 2, it can be observed that, as expected, dead reckoning is the fastest algorithm, followed by KF Post-processed (since measures relative to the transceiver's location were heuristically excluded from the processing) and KF. The B-PR-F framework presented an execution time proportional to the sum of the KF and dead reckoning execution times. This is reasonable, since in the architecture the two estimators were running simultaneously (although the implementation was optimized to avoid recalculations). The A-MCL algorithm presented the highest execution time, which may compromise the on-line performance. It is relevant to salient at this point that the comparison on the execution times described was performed by running the algorithms off-line.

Finally, for the case of the architecture designed, and the experiment performed, the ROV was unimodally connected to a control unit on the sea surface, so the problem of delay and fusion was mitigated. Hence, it remains for future research the evaluation of B-PR-F in delayed measurement scenarios.

## 8. Conclusions

This work proposed a methodology that allowed the system designer to define an ordered arrangement between redundant state estimates, viewed as black-box processes, so their information can be combined robustly in the presence of unmodelled noise.

In the architecture proposed redundant estimation processes are encapsu-

lated in nodes and organized within first-order neighborhoods, according to their properties. The fusion method consisted in a neural network structure named B-PR-N. The model relied on the principle of contextually anticipating the localization signal within the neighborhood, so that estimates were related to the task context, and the confidence on estimates was explicitly represented and evaluated previous to the fusion.

The framework outperformed state-of-the-art solutions such as the KF and the A-MCL algorithms. In relation to the former, B-PR-N was able to dynamically ignore noisy fixes in the fusion process, which resulted in more precise localization estimates. In relation to the later, B-PR-N was able to be flexible to unmodeled noise at a lower computational cost. This shows that the model proposed is a convenient tool for applications in real underwater localization scenarios with ROV architectures. We believe that the principle proposed can also be relevant to related application fields, involving the problem of state estimation from the fusion of redundant information.

Some aspects remained for future research. Firstly, given the robustness obtained in the fusion process, the framework is going to be integrated to a bio-inspired architecture under development in our lab (see Chame et al. [22]), so that the information on the localization is represented in a grid cell neural network. Secondly, additional experiments are going to be designed under multiple behavior profiles, so the performance of the model can be analyzed more in depth. Thirdly, only one target was localized in the experiment, it would be interesting to explore a scenario including multiple targets localization. Fourthly, we believe that the layered representation proposed can be a convenient means to detect anomalous situations, such as sensory momentary degradation, this hypothesis should be studied in a separate research. Finally, an interesting aspect to be explored is the performance of the model for scenarios where measurement fixes are received delayed, which has been reported in some research involving experiments with AUV robots.

## ACKNOWLEDGMENT

This work has been funded by the *Programa Nacional de Pós-Doutorado* (PNPD), CAPES Foundation, Ministry of Education of Brazil, Brasília - DF 700040-020, Brazil.

## References

- [1] L. Paull, S. Saeedi, M. Seto, H. Li, Auv navigation and localization: A review, *IEEE Journal of Oceanic Engineering* 39 (1) (2014) 131–149. doi:10.1109/JOE.2013.2278891.
- [2] E. I. Grøtli, J. Tjønnås, J. Azpiazu, A. A. Monseth, M. Ludvigsen, Towards more autonomous rov operations. Scalable and modular localization with experiment data, *IFAC-PapersOnLine* 49 (23) (2016) 173 – 180. doi:10.1016/j.ifacol.2016.10.339
- [3] H. P. Tan, R. Diamant, W. U. Soh, M. Waldmeyer, A survey of techniques and challenges in underwater localization, *Ocean Engineering* 38 (14) (2011) 1663 – 1676. doi:10.1016/j.oceaneng.2011.07.017.
- [4] J. Luo, Y. Han, L. Fan, Underwater acoustic target tracking: A review, *Sensors* 18 (1).
- [5] L. Drolet, F. Michaud, J. Cote, Adaptable sensor fusion using multiple kalman filters, in: *Proceedings. 2000 IEEE/RSJ International Conference on Intelligent Robots and Systems (IROS 2000)* (Cat. No.00CH37113), Vol. 2, 2000, pp. 1434–1439 vol.2. doi:10.1109/IROS.2000.893222.
- [6] R. K. Van, T. Taher, F. S. Hover, Accurate geo-referencing method for rovs for oceanographic sampling, in: *OCEANS 2010 MTS/IEEE SEATTLE*, 2010, pp. 1–5. doi:10.1109/OCEANS.2010.5664570.
- [7] S. Belchior, R. Neves, L. Taddei, V. Oliveira, Using augmented state kalman filter to localize multi autonomous underwater vehicles, *Journal of the Brazilian Computer Society* 13 (2) (2007) 61–70. doi:10.1007/BF03192410.

- [8] S. Potyagaylo, C. C. Constantinou, G. Georgiades, S. G. Lezou, Asynchronous ukf-based localization of an underwater robotic vehicle for aquaculture inspection operations, in: OCEANS'15 MTS/IEEE Washington, IEEE, 2015, pp. 1–6. doi:10.23919/OCEANS.2015.7404532
- [9] S. Thrun, W. Burgard, D. Fox, Probabilistic Robotics, The MIT Press, Cambridge, Mass., 2005.
- [10] M. Morgado, P. Batista, P. Oliveira, C. Silvestre, Position usbl/dvl sensor-based navigation filter in the presence of unknown ocean currents, *Automatica* 47 (12) (2011) 2604 – 2614. doi:10.1016/j.automatica.2011.09.024.
- [11] X. Gao, X. Zhong, D. You, S. Katayama, Kalman filtering compensated by radial basis function neural network to seam tracking of laser welding, *IEEE Transactions on Control Systems Technology* 21 (5) (2013) 1916–1923. doi:10.1109/TCST.2012.219861.
- [12] S. J. Julier, J. K. Uhlmann, Using covariance intersection for SLAM, *Robotics and Autonomous Systems* 55 (1) (2007) 3 – 20, simultaneous Localisation and Map Building. doi:10.1016/j.robot.2006.06.011.
- [13] A. Sabra, W. k. Fun, Dynamic localization plan for underwater mobile sensor nodes using fuzzy decision support system, in: OCEANS 2017 #8211; Anchorage, 2017, pp. 1–6, ISBN: 978-0-6929-4690-9.
- [14] A. Gopalakrishnan, N. S. Kaisare, S. Narasimhan, Incorporating delayed and infrequent measurements in extended kalman filter based nonlinear state estimation, *Journal of Process Control* 21 (1) (2011) 119 – 129. doi:10.1016/j.jprocont.2010.10.013.
- [15] F. Rida, D. Ribas, E. Hernández, A. Rusu, Usbl/dvl navigation through delayed position fixes, in: 2011 IEEE International Conference on Robotics and Automation, 2011, pp. 2344–2349. doi:10.1109/ICRA.2011.5980110.
- [16] F. Asadi, C. L. Bottasso, Delayed fusion of relative state measurements by extending stochastic cloning via direct kalman filtering, in: Proceedings of

the 16th International Conference on Information Fusion, 2017, pp. 2049–2056, ISBN:978-1-4799-0284-2.

- [17] H. F. Chame, C. Chevallereau, Grounding humanoid visually guided walking: From action-independent to action-oriented knowledge, *Information Sciences* 352–353 (2016) 79 – 97. doi:10.1016/j.ins.2016.02.033.
- [18] M. M. M. Manhães, S. A. Scherer, M. Voss, L. R. Douçet, T. Rauschenbach, UUV simulator: A gazebo-based package for underwater intervention and multi-robot simulation, in: OCEANS 2016 MTS/IEEE Monterey, IEEE, 2016. doi:10.1109/oceans.2016.7761080.
- [19] A. Burguera, Y. González, G. Oliver, *Ti-SLAM: Performing scan matching localization using an imaging sonar*, *Sensors* 12 (6) (2012) 7855–7885. doi:10.3390/s120607855.
- [20] B. D. Lucas, T. Kanade, An iterative image registration technique with an application to stereo vision, in: *Proceedings of the 7th International Joint Conference on Artificial Intelligence - Volume 2*, IJCAI'81, 1981, pp. 674–679.
- [21] H. F. Chame, M. d. S. Machado, S. S. d. C. Botelho, Reliable fusion of black-box estimates of underwater localization, in: IEEE/RSJ International Conference on Intelligent Robots and Systems (IROS), Madrid, Spain, 2018. (Accepted).
- [22] H. F. Chame, P. L. Drews, S. S. C. Botelho, Towards a biologically-inspired model for underwater localization based on sensory-motor coupling, in: 2017 Latin American Robotics Symposium (LARS) and 2017 Brazilian Symposium on Robotics (SBR), 2017, pp. 1–6. doi:10.1109/SBR-LARS-H.2017.815274.

## Appendix A

In this Appendix section the details of the simulation study are summarized. The model parameters are described in Table 3. Distances are expressed in meters and time in seconds. The global mean issued by the network is denoted by  $\bar{\mu}_{(t)}$  (see Eq. (18)). The expected time change for the estimators is denoted by  $\tilde{t}_{i(t)}$ . Reset times  $t_r$  occur when the reliability test, as modeled by Layer R, is satisfactory (see. Eqs.(14), (15), (16)). The initial state of the estimator's covariance matrix  $\Sigma_{ib(t_r)}$  at reset times are set according to the two behavior profiles  $b \in \{1, 2\}$  modeled.

P	E1	E2	E3	E4
$\mu_{i(t_r)}$	$\bar{\mu}_{(t_r)}$	$\bar{\mu}_{(t_r)}$	$\bar{\mu}_{(t_r)}$	$\bar{\mu}_{(t_r)}$
$\mu_{i(t)}$	$\mu_{1(t-1)} + \mathbf{x}_{\text{imu}(t)}$	$\mu_{2(t-1)} + \mathbf{x}_{\text{imu}(t)}$	$\mathbf{x}_{\text{usbl}(t)}$	$\mathbf{x}_{\text{dgps}(t)}$
$\Sigma_{i1(t_r)}$	$10I_{[3]}$	$10000I_{[3]}$	$0.4I_{[3]}$	$0.01I_{[3]}$
$\Sigma_{i2(t_r)}$	$10000I_{[3]}$	$2I_{[3]}$	$0.4I_{[3]}$	$0.01I_{[3]}$
$\Sigma_{i(t)}$	$\Sigma_{1(t-1)} + \hat{\mathbf{X}}_{1(t)}$	$\Sigma_{2(t-1)} + \hat{\mathbf{X}}_{2(t)}$	$\Sigma_{3(t-1)} + \hat{\mathbf{X}}_{3(t)}$	$\Sigma_{4(t-1)} + \hat{\mathbf{X}}_{4(t)}$
$\tilde{t}_{i(t)}$	0.34	0.34	13.61	-

Table 3: Model parameters (P) for the simulation study.

The B-PR-N mode<sup>1</sup>' parameters were set so  $\tau_j = \tilde{t}_{k(t)}^{-1}|k = c_{lb}(j)$  (with  $\tilde{t}_{3(t)} = \tilde{t}_{3(t)}/3$ ),  $\phi_1 = 30^\circ$ ,  $\phi_2 = 13.0$ . The behavior transitions were modeled by setting a threshold of 30 m to altimeter measurements. The system configuration, representing the estimator's reliability along each behavior profile, was set so  $\mathbf{W}^R = \begin{bmatrix} 0.0 & 0.0001 & 2.0 & 10.0 \\ 0.0 & 0.8 & 1.8 & 0.0001 \end{bmatrix}$ .

The UoBL readings  $\mathbf{x}_{\text{usbl}} = \mathbf{x}_{\text{gt}} + \epsilon_1 + \epsilon_2$  are simulated by adding Gaussian noise  $\epsilon_1 \sim \mathcal{N}(0, \sigma_{\epsilon_1}^2)$  to the ground truth value  $\mathbf{x}_{\text{gt}}$ , with  $\sigma_{\epsilon_1}^2 \in [2, 10]$  linearly varying, depending on the relative depth from the transceiver location (which is fixed to the initial coordinate of the simulation, near the water surface); and a non-Gaussian noise  $\epsilon_2$  consisting on arbitrary setting random measurements to large deviations from the reference value. The IMU readings are simulated so  $\ddot{\mathbf{x}}_{\text{imu}} = \ddot{\mathbf{x}}_{\text{gt}} + \epsilon_3$ , with  $\epsilon_3 \sim \mathcal{N}(0, 0.75)$ . The DVL readings are obtained by

$\dot{\mathbf{x}}_{\text{dvl}} = \dot{\mathbf{x}}_{\text{gt}} + \epsilon_4$ , with  $\epsilon_4 \sim \mathcal{N}(0, 0.25)$ . The DGPS readings are generated such that  $\mathbf{x}_{\text{dgps}} = \mathbf{x}_{\text{gt}} + \epsilon_5$ , with  $\epsilon_5 \sim \mathcal{N}(0, 0.01)$ .  $\hat{\mathbf{X}}_{i(t)} = \text{diag}(|\mathbf{x}_{\text{sc}}(t)|)$ , with  $\hat{\mathbf{x}}_{i(t)} \in \{\mathbf{x}_{\text{imu}}(t), \mathbf{x}_{\text{dvl}}(t), \mathbf{x}_{\text{usbl}}(t), \mathbf{x}_{\text{dgps}}(t)\}$ .

## Appendix B

In this Appendix section additional information about the experimental study is presented. The model parameters set are described in Table 4. Distances are expressed in m and time in sec. The network global estimate is denoted by  $\bar{\mu}_{(t)}$ , the expected estimator time range is denoted by  $\tilde{\delta t}_{i(t)}$ , and  $t_r$  is the reset time. The vector  $\mathbf{x}_{\text{sc}(t)} = [\Delta x \ \Delta \eta]^\top$  is the scan-matching motion estimation. The selected parameters were set empirically by analyzing the captured dataset off-line.

P	Estimator 1	Estimator 2	B-PR-N
$\mu_{i(t_r)}$	$\bar{\mu}_{(t_r)}$	$\mu_{(\cdot,\cdot)}$	-
$\mu_{i(t)}$	$\mu_{1(t-1)} + \mathbf{x}_{\text{sc}}(t)$	$\mu_{-(t t-1)}$ , Eq.(25)	-
$\Sigma_{i(t_r)}$	$8.0\mathbf{I}_{[2]}$	$0.2\mathbf{I}_{[2]}$	-
$\Sigma_{i(t)}$	$\Sigma_{1(t-1)} + \text{diag}( \mathbf{x}_{\text{sc}}(t) )$	$\tilde{\mathbf{P}}_{(t t-1)}$ , Eq.(25)	-
$\tilde{\delta t}_{i(t)}$	0.18	2.52	-
-	$\sigma_{\text{odom}} = [0.5 \ 0.5]$	$\sigma_{\text{usbl}} = [0.1 \ 0.1]^\top$	-
$\tau_1$	-	-	$10\tilde{\delta t}_{2(t)}$
$\phi_1$	-	-	0.2
$\phi_2$	-	-	13.0
$\mathbf{W}^x$	-	-	$[0.2, 0.8]^\top$

Table 4 Model parameters (P) for the experimental study.

The sources implementation of the simulation and the experimental study in GNU Octave version 4.0.0 can be downloaded from the following Github address: <https://github.com/henferch/B-PR-F>

**ACCEPTED MANUSCRIPT**  
**Authors Biography Document**

**Manuscript:** Neural network for black-box fusion of underwater robot localization under unmodeled noise

**Dr. Hendry Ferreira Chame** is Graduated in Psychology in 2004 from Universidad Central de Venezuela (UCV), Caracas, Venezuela, and in Computer Science in 2008 from UCV. He has received a Master degree in Instructional Psychology in 2007 from UCV, and a Master degree in robotics in 2012 from the Ecole Centrale de Nantes (ECN), Nantes, France. He obtained his PhD degree in robotics in 2016 from the ECN. His research interests include cognitive robotics, artificial intelligence, embodied cognition, and machine vision, among others.

**Msc. Matheus Machado dos Santos** is Graduated (2013) and Master(2015) in Computer Engineering from the Universidade Federal do Rio Grande, FURG. Nowadays he is a Ph.D. student at FURG and acts on the following topics: Petri Nets, Multi-Agent Systems, Systems Based on Knowledge, Computer Vision, Acoustic Images, Optical Acoustical Systems, Simultaneous Localisation and Mapping, Mobile Robotics.

**Prof. Dr. Silvia Silvia da Costa Botelho** is graduated in Electric Engineering in 1991 and received her Master degrees (1994) in Computer Science from the Federal University of Rio Grande do Sul – UFRGS. Her Doctorate (2000) was in Robotic from Laboratoire d'Analyse et d'Architecture de Systèmes - LAAS/CNRS, France. Her Ph.D. Thesis was "An Architecture for Multi-robot Cooperation" and her advisor was Dr. Rachid Alami. In August 1992 she joined the Universidade Federal do Rio Grande, FURG, where nowadays she acts as director of the Center of Computational Science- C3.

**Manuscript:** Neural network for black-box fusion of underwater robot localization under unmodeled noise

**Dr. Hendry Ferreira Chame**



**Msc. Matheus Machado dos Santos**



**Pr. Dr. Sílvia Silva da Costa Botelho**



**localization under unmodeled noise**

Hendry Ferreira Chame, Matheus Machado dos Santos, Sílvia Silva da Costa Botelho

**Highlights**

- We study reliable and efficient approaches for autonomous underwater robot localization.
- We assume that black-box redundant estimates are available to the system under distinct scenarios.
- We propose a neural network framework which heuristically fuses information based on the principle of information anticipation.
- We illustrate in a virtual environment how our framework handles unmodeled noise.
- Experimental results show our model outperformed KF and A-MCL in the localization task.